A Portable Sensor Device for Real-Time Viscosity Measurement of Lubricating Oil

Chengze Liu[1,2], Chenxing Sheng[1,2], Xiang Rao[1,2], Bo Zhao[3], Zhijun Chen[2,*]
[1]State Key Laboratory of Maritime Technology and Safety, Wuhan University of Technology, Heping Rd. 1080, Wuhan, 430063, China
[2]School of Naval Architecture, Ocean and Energy Power Engineering, Wuhan University of Technology, Heping Rd. 1080, Wuhan, 430063, China
[3]Wuhan Second Ship Design and Research Institute, Zhongshan Rd. 450, Wuhan, 430200, China
*liucz@whut.edu.cn; scx01@whut.edu.cn; rxiang@whut.edu.cn; bahazhao@163.com; *czj@whut.edu.cn*

***Abstract*—The viscosity of lubricating oil is a critical indicator for assessing both its performance and degradation, and it plays a vital role in the monitoring of equipment condition. To meet the need for portable and automated viscosity measurement of lubricant oil in engineering applications, this paper presents a novel device based on Newton's law of viscosity and strain-based sensing principles. The device detects the minute deflection of a cantilever beam under fluid impact and converts the induced strain into an electrical signal via bonded strain gauges to measure viscosity. Then, a finite element simulation was performed to optimise the structure of the cantilever beam and determine the placement of the strain gauges. Experimental validation using glycerol-water mixtures and 4050 lubricating oil demonstrated that the device exhibited a strong linear correlation between its output and reference viscosity values, and that it maintained high measurement accuracy and strong applicability under critical temperature conditions, such as the ISO standard temperature of 40 °C, as well as in high-viscosity regimes. Finally, the comparison between the proposed device and the representative commercial products indicated that the device is well suited for on-site industrial viscosity measurement requiring portability, automation, and cost-effectiveness. This work provides a technical reference and practical foundation for viscosity measurement in engineering applications.**

***Index Terms*—Portable device; Sensor technology; Lubricating oil viscosity; Online measurement.**

I. INTRODUCTION

Lubricating oil, often referred to as the "blood" of mechanical systems, not only provides essential functions such as cooling, sealing, prevention of corrosion and rust, and removal of contaminants, but also carries valuable information on the condition of the equipment [1]. Over extended use, its performance gradually deteriorates as a result of oxidation, contamination, and additive depletion. Continued use of degraded oil can lead to lubrication failure, increased friction, and eventually mechanical breakdown. As one of the key parameters for evaluating oil performance, viscosity plays a central role [2], [3]: excessive viscosity reduces flow efficiency, while insufficient viscosity prevents the formation of a stable lubricating film, significantly increasing the risk of wear. Therefore, viscosity monitoring is of great significance to ensure equipment reliability and to support informed maintenance decisions.

Currently, viscosity measurement techniques are generally divided into two categories: offline and online [4]. Offline techniques, such as the capillary method, rotational method, and falling ball method, are widely used in laboratory environments due to their robust theoretical basis and high measurement precision [5]. However, they typically require manual operation, involve complex procedures, and have a long response time [6]. Moreover, the need for sample extraction and external laboratory analysis limits their applicability in complex industrial conditions. To overcome these limitations, online viscosity monitoring has gained increasing attention. Based on their working principles, online techniques can be further classified into three main types: vibration-based, wave propagation-based, and displacement-based methods [7], [8].

Vibration-based methods excite sensing elements to generate periodic oscillations within the fluid, and determine fluid viscosity by monitoring variations in their vibrational parameters, such as amplitude and resonant frequency [9], [10]. A typical example is the piezoelectric sensor. For example, Lu, Hou, Zhang, Tong, Zhao, and Cheng [11] used the resonance frequency and quality factor (Q factor) of PVDF membranes to determine viscosity. Yanaseko, Sato, Kuboki, Mossi, and Asanuma [12] developed a piezoelectric ceramic composite reinforced with a metal matrix and extracted oil viscosity information by analysing variations in damping amplitude and resonance frequency. Although these sensors offer high sensitivity and a compact design, they still face challenges such as low viscosity range, lack of analytical models, and complex calibration procedures.

Wave propagation-based methods analyse viscosity by observing how ultrasonic or shear waves propagate through fluids. Since fluid viscosity affects wave attenuation and phase velocity, it can be inferred from spectral response or echo characteristics. Yu, Liang, and Yuandong [13]

Manuscript received 2 September, 2025; accepted 21 October, 2025.
This research was supported by the National Natural Science Foundation of China under Grant No. 52372361; the Key Laboratory of Marine Power Engineering and Technology of the Ministry of Transport under Grant No. KLMPET2023-01.

employed capacitive micromachined ultrasonic transducers (CMUTs) to transmit and receive echo signals, using frequency shifts to characterise viscosity. Schirru, Li, Cadeddu, and Dwyer-Joyce [14] developed an acoustic model for wave propagation in viscoelastic fluids and used shear wave reflectivity as a viscosity indicator. Although this approach allows for noncontact and rapid viscosity measurement, it typically requires reflectors, large fluid chambers, and sufficient sample volumes. Moreover, as structural dimensions increase, higher demands are placed on sensor layout and data processing capabilities.

In displacement-based methods, the mechanical behaviour of structural elements (e.g., deformation, deflection, or displacement velocity) is monitored under fluid-induced forces to estimate fluid viscosity. When these structures are analysed as they respond to flow, a measurable correlation between hydrodynamic loading and viscosity can be established. Owing to their structural simplicity and intuitive sensing principle, such methods are widely employed in the design of fluidic microsensors. Common structures include microcantilever beams [15], micromembrane [16], and invasive probes [17]. In recent years, optical fibers have been introduced into displacement measurement because of their excellent resistance to electromagnetic interference. Gomes, Kobelke, Bierlich, Schuster, Bartelt, and Frazao [18] developed a miniaturized interferometric probe based on a hollow capillary tube, where fluid viscosity was inferred from the evacuation velocity of the gas-liquid interface during probe withdrawal. Similarly, droplet travel time across two decladded regions of a fiber-fixed probe has been explored as a viscosity sensing mechanism [19]. However, these systems require dedicated demodulation equipment and their performance can be influenced by factors such as temperature-induced coupling effects.

In summary, although existing online viscosity detection technologies have made significant progress, they still face limitations in terms of rapid deployment, structural simplicity, and controllability of implementation complexity, particularly in cost-sensitive engineering scenarios. Therefore, this paper presents a portable and automated viscosity measurement device for lubricating oil. The system consists mainly of a spiral flow tube, a temperature control module, and a cantilever that serves as a viscosity sensor. As the fluid flows, its impact on the cantilever induces measurable deformation. Since fluids with different viscosities generate different deformation signals of varying magnitudes, these data can be used to establish a quantitative relationship between viscosity and mechanical response. In addition, the temperature control module can ensure a stable testing environment. Viscosity measurement was performed on glycerol-water mixtures of various concentrations and 4050 aviation lubricating oil under multiple temperature conditions. The results were compared with those of a standard viscometer to verify the device's performance. In addition, a comparative analysis with the main commercial products was carried out to evaluate their potential and value for engineering applications.

The remaining parts of the paper are organised as follows. Section II introduces the design and working principle of the device. Section III describes and analyses the experimental validation results of the proposed device. Section IV provides the conclusions.

II. SENSOR DESIGN AND OPERATION PRINCIPLE

A. Structure Design

The structure and physical appearance of the viscosity measurement device are illustrated in Fig. 1, which includes a 3D model, a top view diagram, and a photograph of the physical prototype. The device is organised into three functional layers: the outer layer, the heating layer, and the inner layer. The outer layer is filled with thermal insulation material to minimise heat loss and maintain the temperature stability in the internal area.

The heating layer contains the spiral tube immersed in heat-transfer oil, along with an immersion heater, a motor-driven impeller, and four temperature sensors. It serves the dual purpose of maintaining laminar flow inside the spiral tube under regulated flow conditions and heating the test fluid until the outlet temperature reaches the desired value. Heat is supplied by the immersion heater, the impeller improves convective heat transfer in the oil bath, and the temperature sensors provide real-time feedback for the proportional-integral-derivative (PID)-controlled heating system. The flow velocity is determined by the pump. According to previous research by the group [20], under the present configuration laminar flow is ensured when the mean velocity is below 0.1 m/s, and the outlet temperature, the inlet temperature, and the ambient temperature satisfy the relationship given in (1)

$$T_{out} = 0.3133T_{in} + 0.6874T_{amb}, \tag{1}$$

where T_{out} is the outlet temperature, T_{in} is the inlet temperature, and T_{amb} is the ambient temperature. Given a known T_{in}, the controller adjusts T_{amb} so that a user-specified target T_{out} is achieved.

The inner layer is dedicated to the measurement of viscosity. The viscosity sensor employs a cantilever structure mounted at the outlet of the tube. As the fluid exits the channel, it strikes the free end of the cantilever, causing measurable deflection that is detected by strain gauges bonded to the surface of the beam. Further details of the sensing principle are provided in the next subsection.

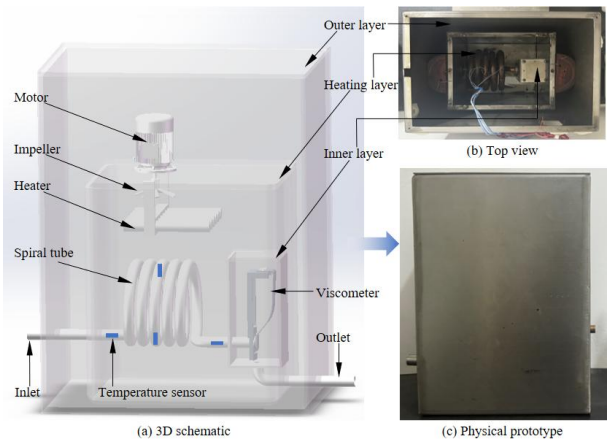

Fig. 1. Structural design of the viscosity measurement device: (a) 3D schematic; (b) Top view; (c) Physical prototype.

The complete measurement workflow is shown in Fig. 2. First, the user sets the initial fluid temperature and the target detection temperature. On the basis of these inputs, the system calculates the required ambient heating temperature. The PID-controlled heating module then adjusts the heater output to raise the ambient temperature, maintaining continuous heating until the target value is reached and thermal equilibrium is established. Once the temperature stabilises, the pump is activated to deliver the test fluid to the spiral tube. As the fluid flows through the tube, it is heated to the specified temperature before exiting the outlet and striking the free end of the cantilever beam, causing measurable deformation. The signal processing unit converts this deformation signal into a viscosity value, which is recorded and displayed in real time. After impact, the fluid is discharged from the outlet under gravity and collected for reuse.

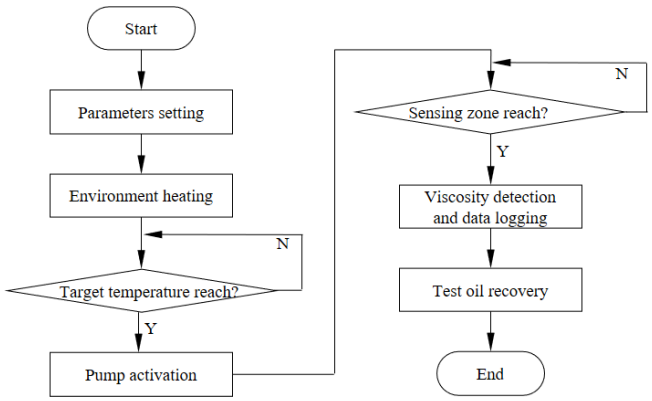

Fig. 2. Operational workflow of the viscosity measurement process.

To provide a more comprehensive perspective, Fig. 3 presents the overall system architecture and signal flow, showing the fluid path from the sample container to the sensing zone, as well as the signal chain from acquisition to processing and display.

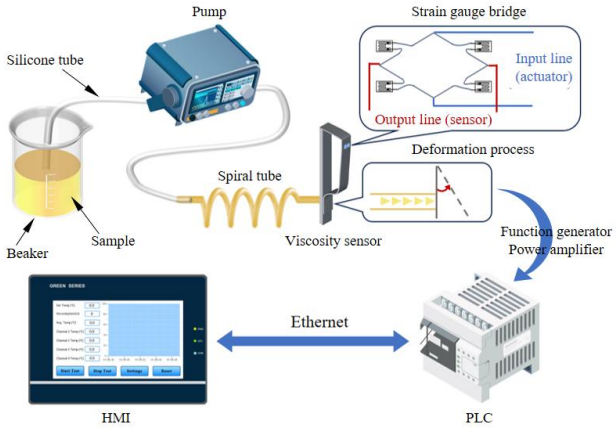

Fig. 3. Overall system architecture and signal flow.

B. *Measurement Principle*

Viscosity is an intrinsic property of fluids, manifesting itself as shear stress when adjacent layers move relative to one another. An example is the couette flow between two parallel plates, as shown in Fig. 4, where a viscous fluid fills the gap, the lower plate remains stationary, and the upper plate moves at a constant velocity *U*. As a result of the no-slip boundary condition, the fluid layer in contact with each plate moves at the same speed as that plate.

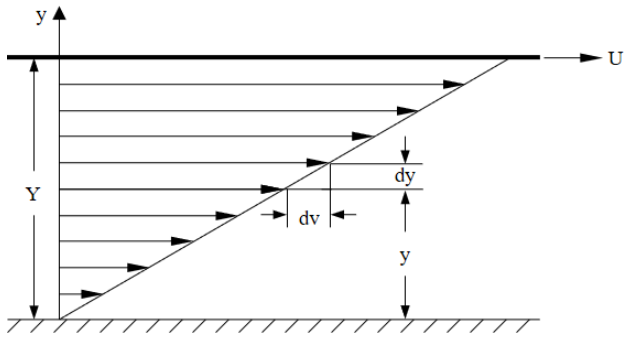

Fig. 4. Illustration of viscous behaviour in fluids.

Under steady, incompressible, laminar conditions without a pressure gradient, the velocity varies uniformly from 0 to *U*, creating a constant velocity gradient across the gap. According to Newton's law of viscosity, the shear stress is proportional to the velocity gradient, as described by

$$\tau = \mu \frac{dv}{dy}, \tag{2}$$

where τ is the shear stress, μ is the fluid viscosity, v is the local flow velocity, y is coordinate normal to the plates. For a surface of area A in contact with the flow, the corresponding viscous force is given by

$$F = \tau A. \tag{3}$$

In the present device, as the fluid exits the spiral tube, it strikes the free end of the cantilever beam. The total force F exerted on the beam can be decomposed into two components

$$F = F_1 + F_2, \tag{4}$$

where F_1 is the dynamic pressure force generated by the flow velocity, and F_2 is the viscous force described by (3). The dynamic pressure force is given by

$$F_1 = \frac{1}{2} C_d \rho A V^2, \tag{5}$$

where C_d is the drag coefficient, ρ is the fluid density, A is the projected frontal area of the beam, and V is the average flow velocity. At high flow velocities, F_1 is the dominant component. As the velocity decreases, the contribution of F_2 becomes more significant. In the low-velocity regime, F is primarily determined by the viscous component and thus scales linearly with the fluid viscosity μ.

The applied force F causes the cantilever beam to undergo bending deformation. According to Euler-Bernoulli beam theory, the surface strain at a distance l from the point of load is given by

$$\varepsilon = \frac{6Fl}{Ebh^2}, \tag{6}$$

where E is the Young modulus of the beam material, b and h are the width and thickness of the beam, respectively.

The strain can be converted into a resistance change ΔR using the bonded strain gauges

$$\frac{\Delta R}{R} = \delta\varepsilon, \tag{7}$$

where δ is the gauge factor and R is the nominal resistance of the strain gauge. The strain gauges are connected on a Wheatstone bridge. When the resistance changes, the bridge output voltage can be expressed as

$$\Delta U = \frac{U}{4}\delta\left(\varepsilon_1 - \varepsilon_2 + \varepsilon_3 - \varepsilon_4\right), \tag{8}$$

where U is the excitation voltage, and ε_i is the strain in each arm of the bridge. Since U is directly related to the strain, and the strain is induced by the external load F, the measured voltage serves as an indicator of the applied force. In the low-velocity regime, this force is mostly caused by viscous effects and varies linearly with the fluid viscosity μ. Therefore, after calibration, the device can determine the viscosity in real time from the measured voltage signal.

C. *Viscosity Sensor Optimisation and Fabrication*

The viscosity sensor, as the core component of the measurement device, has its performance largely determined by the ability of the cantilever beam to respond to small external forces. Stainless steel was chosen as the beam substrate due to its high elastic modulus, excellent corrosion resistance, low temperature drift, and minimal elastic hysteresis [21]. To improve the beam strain response without compromising its overall strength and stability, a localised reduction in thickness was introduced near the fixed end.

Based on the expected operating conditions, finite element simulations were performed to compare the stress and displacement distributions of the original model (uniform thickness) and the optimised model (locally thinned) under load. In the simulations, the top surface of the beam was fixed and a concentrated load of 1 N was applied near the free end in the flow-facing direction to represent the impact force exerted by the fluid. The material properties were set to a Young's modulus of 1.93×10^{11} Pa, a density of 7750 kg/m^3, and a Poisson's ratio of 0.31. Tetrahedral solid elements were used for meshing, with local refinement in the loading and stress concentration zones to improve accuracy. All key structural parameters were kept identical between the two models, with both beams having a width of 14 mm and a thickness of 1 mm, except that the optimised model had a locally reduced thickness in the thinned region.

Simulation results in Fig. 5 show that, under the same applied load, the optimised model achieved a maximum tip displacement of 257.13 µm, which is markedly higher than the 72.285 µm observed in the original model. It demonstrates that the localised thickness reduction significantly enhances the deformation response of the beam. Figure 6 shows the corresponding stress distributions. The optimised beam exhibited a maximum strain of 0.097193, more than twice that of the original model, with the strain concentration clearly localised in the thinned section. Such strain localisation not only improves measurement sensitivity, but also precisely identifies the optimal location for strain gauge placement.

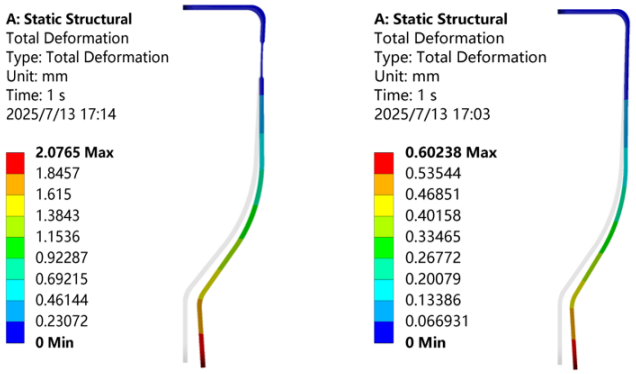

(a) Optimized model (b) Original model

Fig. 5. Displacement distribution of the cantilever beam: (a) Optimised model; (b) Original model.

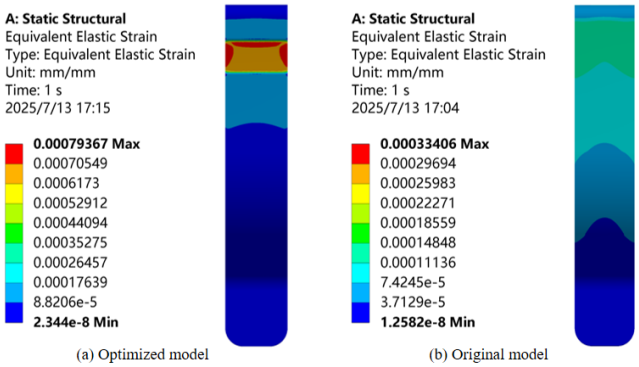

(a) Optimized model (b) Original model

Fig. 6. Stress distribution of the cantilever beam: (a) Optimised model; (b) Original model.

Figure 7 presents a photograph of the fabricated viscosity sensor mounted on the brass support.

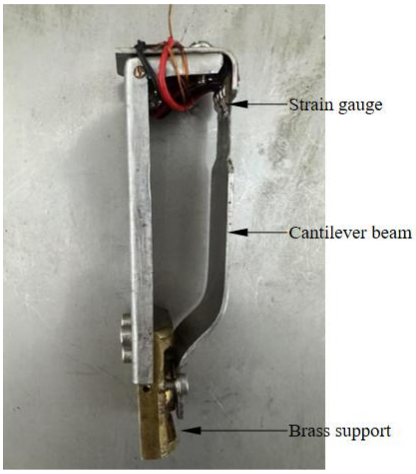

Fig. 7. Physical prototype of the optimised viscosity sensor.

III. EXPERIMENTAL RESULTS AND DISCUSSION

A. *Experimental Setting*

Two types of glycerol-water mixtures with different volume concentrations (90 %: 10 % water and 90 % glycerol; 80 %: 20 % water and 80 % glycerol) and 4050 aviation lubricating oil were selected as test samples. The glycerol-water mixtures exhibit Newtonian fluid behaviour, are readily available, and can be formulated with adjustable viscosity by varying the mixing ratio to cover the range of the most commonly used lubricating oil. The 4050 oil is a high-

performance lubricant, chosen to represent real working fluids in practical engineering applications.

The glycerol-water mixtures were prepared manually by measuring the required volumes of glycerol and water with a graduated cylinder, transferring them into a clean beaker, and stirring steadily with a glass rod for five minutes until a transparent, homogeneous solution was obtained. The mixtures were then allowed to stand for 10 minutes to release any residual bubbles and stabilise the temperature. All viscosity tests were completed within 30 minutes of preparation. The 4050 oil was tested directly as received from the manufacturer without further processing.

To maintain stable laminar flow in the spiral tube and ensure that the outlet temperature reaches the target value, an intelligent peristaltic pump was used to precisely control the flow velocity. Based on the flow velocity recommendations in [20], the pump speed was set to 80 r/min. The system sampling frequency was 10 Hz, and each experiment was repeated eight times, with the average value taken to minimise random errors. Viscosity tests were conducted at outlet temperatures of 30 °C, 40 °C, 50 °C, 60 °C, and 70 °C, corresponding to the typical operating temperature range of most lubricating oils.

B. Calibration Curve

To create a relationship between the device output and fluid viscosity, six additional glycerol-water mixtures with different concentrations were prepared following the same procedure described in Section III-A. These samples were not among the three test fluids described above. Their viscosities at 40 °C, measured using a SYD-265C viscometer, were 196.768 mm^2/s, 124.989 mm^2/s, 76.448 mm^2/s, 47.806 mm^2/s, 18.167 mm^2/s, and 6.390 mm^2/s.

When fluids of different viscosities exited the spiral tube and struck the viscosity sensor, the Wheatstone bridge converted the resulting strain in the cantilever beam into an analogue voltage signal, which was then digitised by the internal A/D module of the PLC. Figure 8 displays the calibration curve, with the x-axis representing the values of the digital signal and the y-axis representing the standard viscosities that correspond. The result demonstrates a strong linear correlation between these two variables, consistent with the theoretical expectation, confirming the feasibility of the proposed method under the present system configuration.

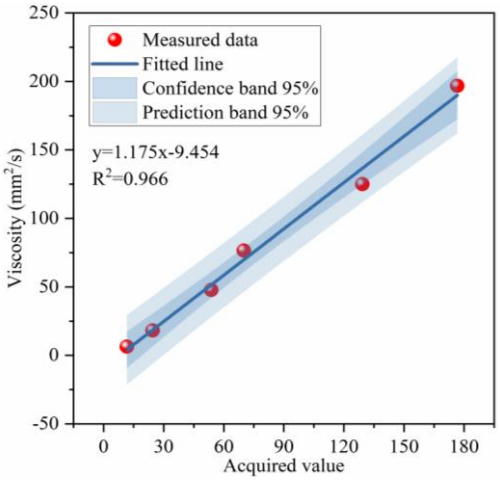

Fig. 8. Calibration curve between the acquired value and the standard kinematic viscosity.

C. Signal Response Characteristics

Figure 9 illustrates the digitised output signal of the viscosity sensor for three test samples throughout the measurement cycle at an outlet temperature of 30 °C. The signal response process can be divided into three stages:

1. Stage 1: Before the fluid reaches the spiral tube outlet, the cantilever beam is not subjected to external load, and the signal remains at the baseline level.
2. Stage 2: Once the fluid leaves the spiral tube and strikes the cantilever beam, the sensor output increases sharply in the primary response interval, and the signal amplitude remains at a high level with noticeable fluctuations over time.
3. Stage 3: As the fluid supply is nearly exhausted, the load is removed, the cantilever beam returns to equilibrium, and the signal gradually falls back to the baseline.

It should be noted that the start and end of Stage II can both be affected by flow-related disturbances, such as entrained bubbles or backflow during the initial period and intermittent supply at the end, resulting in deviations of the sensor response from the actual viscosity. To ensure measurement accuracy, a stable signal interval within Stage II (highlighted by the red box in Fig. 9(a)) was selected as the valid data for viscosity calculation. The start and end times of this interval can be determined by visual observation of the fluid state at the outlet: the user manually triggered the start time once the outflow stabilised and the end time before the sample was exhausted.

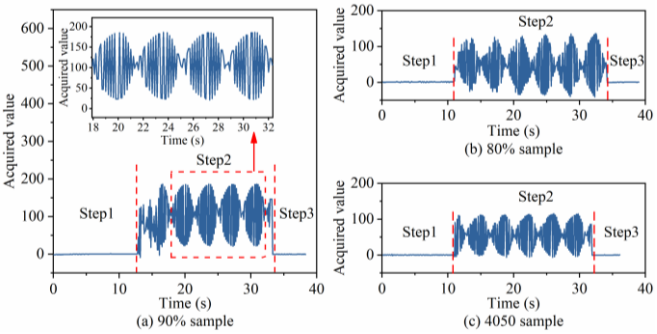

Fig. 9. Viscosity sensor signals for three test samples at 30 °C: (a) 90 % sample; (b) 80 % sample; (c) 4050 sample.

The red-boxed signal segment exhibited clear periodic fluctuation in the time domain. Fast Fourier transform (FFT) analysis was used to identity its frequency distribution, the result is presented in Fig. 10(b). The dominant frequency was observed at 4.589 Hz. The peristaltic pump used in the experiment has a three-roller configuration and was operated at 1.33 Hz (80 r/min), corresponding to a theoretical pulsation frequency of about 4 Hz. It is close to the measured value. The deviation may be attributed to factors such as system response delay, elastic deformation of the tubing, or fluid inertia.

FFT was also performed on the time-domain signals of the 80 % glycerol-water mixture and the 4050 oil at 30 °C. Figures 10(c) and 10(d) present the dominant frequency components for these two samples, with peaks at 4.555 Hz and 4.590 Hz, respectively. Compared to the result for the 90 % mixture, all three samples exhibited nearly identical dominant frequencies. It suggests that periodic fluctuation is primarily determined by the operating characteristics of the

peristaltic pump rather than by the rheological properties of the fluids. The mean amplitude of the red-boxed segment was used for viscosity calculation, which helps suppress pulsation-induced disturbances from the pump and improves the stability and accuracy of the measurement.

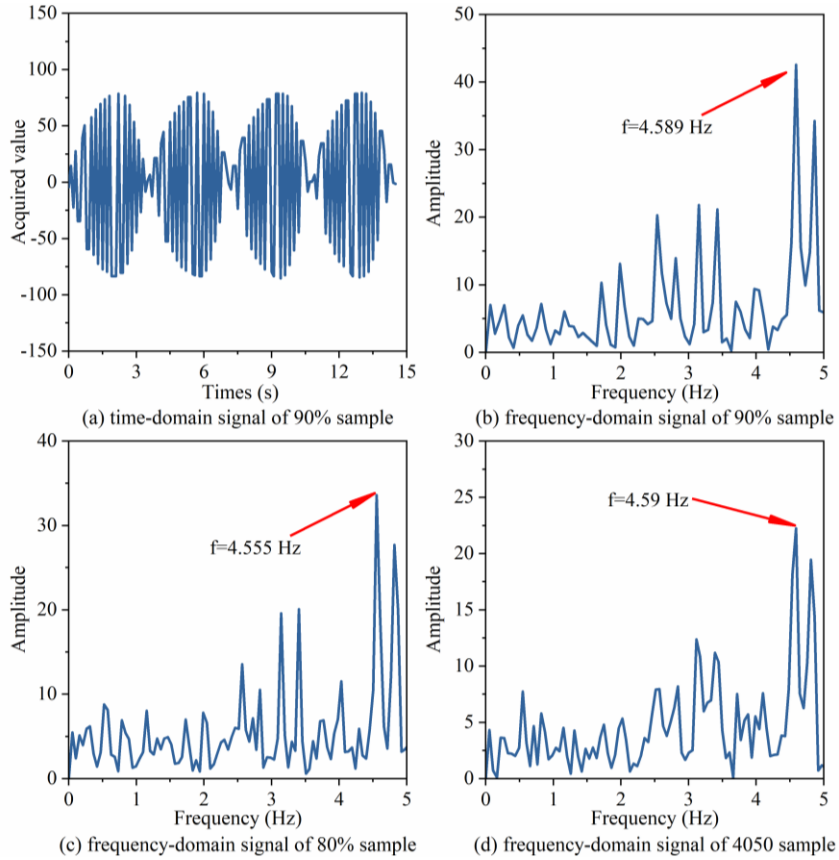

Fig. 10. Time- and frequency-domain analysis of viscosity signals: (a) Time-domain signal of 90 % sample; (b) Frequency-domain signal of 90 % sample; (c) Frequency-domain signal of 80 % sample; (d) Frequency-domain signal of 4050 sample.

D. Viscosity-Temperature Curve and Error Analysis

It can be seen from Fig. 11 that the viscosity of all the three samples decreases with increasing temperature in the range of 30 °C–70 °C, following a trend consistent with the Andrade model, which describes the exponential dependence of fluid viscosity on absolute temperature. The repeatability error at each measurement point was maintained within 12.2 %, and no noticeable systematic deviation was observed between different temperatures or sample types, indicating that the device provided stable and consistent output under controlled conditions.

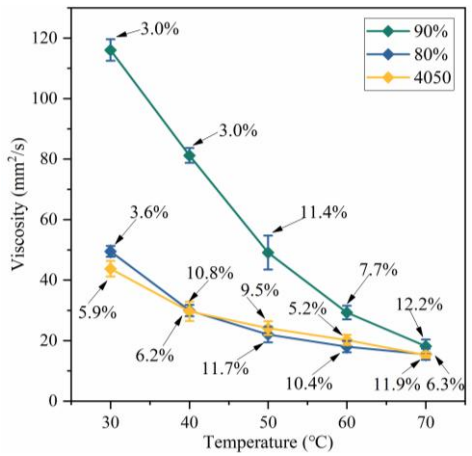

Fig. 11. Effect of temperature on viscosity for different samples.

The measured viscosity values were compared with the standard values obtained from the SYD-265C viscometer, and the results are summarized in Table I. The temperature of 40 °C is both the ISO-specified reference test condition and a representative long-term operating range for lubricating oil. At this temperature, the measurement errors for the 90 % mixture, the 80 % mixture, and the 4050 lubricating oil were 5.2 %, 7.6 %, and 6.3 %, respectively, all well within 8 %. This indicates that the device can achieve high measurement accuracy under this critical condition. Therefore, this device can adjust test samples to 40 °C for viscosity analysis such as standardised condition assessment in practical applications.

To further evaluate the performance of the device at different viscosity levels, the test data were grouped into two ranges according to the standard viscosity values.

1. High-viscosity range (> 30 mm²/s): the deviations of the measured values from the standard values were generally small, with the maximum relative error not exceeding 10.2 %. The device can provide good measurement accuracy and applicability for high-viscosity fluids.
2. Medium-to-low viscosity range (8 mm²/s–30 mm²/s): As the viscosity of the samples decreased, the relative errors increased markedly, with the 80 % mixture at 70 °C exhibiting the largest measurement error of 80.1 %. It was primarily attributed to the low signal resolution of the current device, which limits its ability to distinguish small differences between similar viscosities. Absolute

deviations in all tests ranged from 1 mm²/s to 8 mm²/s. These deviations correspond to a relatively higher proportion of the viscosity values in low-viscosity samples than in high-viscosity samples, thereby resulting in markedly higher relative errors in the former. Furthermore, droplets were observed on the inner wall of the outlet silicone tubing during high-temperature tests, which may have originated from water evaporation within the mixture and/or condensation of ambient moisture. The changes could alter the composition of the samples, which would affect the measurement results and ultimately increase the measurement error. Compared to the standard viscometer, this effect is more pronounced in the present device because it requires a larger sample volume and operates under flow conditions closer to real applications. Notably, this phenomenon was not observed in the 4050 lubricating oil tests, as the low volatility of the oil and the high thermal stability ensured that its composition and physical state remained essentially unchanged during the test.

TABLE I. COMPARISON BETWEEN MEASURED AND STANDARD VISCOSITY VALUES.

Sample	Temperature (°C)	Measured value (mm^2/s)	Standard value (mm^2/s)	Deviation (mm^2/s)	Relative error (%)
90 %	30	116.033	108.420	7.613	7.0
	40	81.199	77.149	4.050	5.2
	50	49.090	45.366	3.724	8.2
	60	30.609	28.882	1.726	6.0
	70	18.476	16.296	2.181	13.4
80 %	30	51.388	56.371	4.983	8.8
	40	31.769	34.381	2.612	7.6
	50	22.008	16.303	5.705	35.0
	60	17.083	11.982	5.101	42.6
	70	15.468	8.589	6.878	80.1
4050	30	43.781	41.009	2.773	6.8
	40	29.657	27.900	1.757	6.3
	50	24.129	18.206	5.923	32.5
	60	20.968	13.141	7.827	59.6
	70	15.224	10.159	5.065	49.9

E. Comparison Analysis

Table II summarizes a brief comparison between the proposed device and several representative commercial viscosity measurement devices. The SYD-265C, TP625, and A1010, all based on the capillary method, are typical offline testing devices that offer high accuracy and good repeatability but are based on manual operation and are large, making them unsuitable for field conditions. The SVM 1101, launched by Anton Paar, is a representative example of automated viscosity measurement, characterised by compact size, high accuracy, and simultaneous multiparameter detection. However, its high costs limit its wider adoption in practice. In contrast, the device developed in this study can meet the basic measurement requirements for high-viscosity oil and has significant advantages in portability and cost-effectiveness. For example, it has dimensions of 250 mm×150 mm×310 mm and weighs 8 kg, integrates automated measurement process, and has a manufacturing cost substantially lower than that of comparable products. With these features, the device is well suited for engineering applications that demand low cost, ease of operation, and flexible deployment.

TABLE II. COMPARISON BETWEEN THE PROPOSED DEVICE AND THE REPRESENTATIVE COMMERCIAL DEVICES.

Brand	Model	Price (CNY/unit)	Specifications
Anton Paar [22]	SVM1101	180,000	Viscosity range: 0.3 mm²/s–1,000 mm²/s; Temperature: 15 °C–100 °C; Operation process: Automatic; Weight: 6.6 kg; Dimensions(L×W×H): 365 mm×330 mm×205 mm.
Delite [23]	A1010	15,000	Viscosity range: Determined by the inner diameter of the equipped capillary tube; Temperature: Ambient to 120 °C; Operation process: Manual; Weight: 18.4 kg; Dimensions(L×W×H): 545 mm×370 mm×500 mm.
Changji [24]	SYD-265C	8,000	Viscosity range: Determined by the inner diameter of the equipped capillary tube; Temperature range: Ambient to 100 °C; Operation process: Manual; Weight: 20.5 kg; Dimensions(L×W×H): 530 mm×400 mm×670 mm.
Timepower [25]	TP625	20,000	Viscosity range: Determined by the inner diameter of the equipped capillary tube; Temperature range: Ambient to 160 °C; Operation process: Manual; Weight: 20 kg; Dimensions(L×W×H): 400 mm×400 mm×620 mm.
Proposed device		2,400	Viscosity range: 30 mm²/s–120 mm²/s; Temperature range: Ambient to 100 °C; Operation process: Automatic; Weight: 8 kg; Dimensions(L×W×H): 250 mm×150 mm×310 mm.

Based on the test results, the device has limited performance at low viscosities. Future research could focus on the following three directions.

1. The sensing and signal processing scheme could be enhanced by incorporating high-sensitivity strain gauges, high-resolution analogue-to-digital converters, and precision front-end circuits, together with advanced signal processing strategies, to improve the extraction of weak deformation signals under low-viscosity conditions.
2. The structural parameters of the cantilever beam could be optimised through fluid-structure interaction simulations to increase its response amplitude to variations in viscous forces.
3. The influence of external parameters such as flow rate on measurement results could be examined, with corresponding compensation models developed to improve the accuracy and adaptability of the device.

IV. CONCLUSIONS

This study developed a portable, compact, and low-cost device for measuring the viscosity of lubricating oil, which consists of a spiral tube, a temperature control module, and a cantilever beam with strain gauges. During operation, the cantilever beam deflects under the impact of the flowing fluid, and the resulting strain is converted into electrical signals for the estimation of the viscosity. To improve sensitivity, the beam was locally thinned and finite element simulation was conducted to optimise the placement of the strain gauges. Six glycerol-water mixtures of different viscosities were used to establish a linear correlation between the device output and the reference values, while time- and frequency-domain analyses were applied to extract the valid signal segment to improve the stability and accuracy of the measurement. The performance experiment using 90 % and 80 % glycerol-water mixtures and 4050 lubricating oil found:

– The repeatability error was within 12.2 %;

– The relative errors were 5.2 %, 7.6 %, and 6.3 % at 40 °C, respectively;

– The maximum relative error in the high-viscosity range (30 mm²/s–120 mm²/s) was limited to 10.2 %.

The results show that, under the present controlled conditions, the device can provide stable and accurate outputs at ISO standard temperature and high-viscosity levels. By combining the comparative analysis, it can be concluded that the device offers significant advantages for field applications, particularly in rapid deployment, cost-effectiveness, and operational efficiency. Future work will focus on enhancing sensing and signal processing capabilities, optimising sensor structural design, and performing multifactor coupling analyses, to improve the device's ability to detect weak signals and its measurement accuracy across a broader viscosity range.

CONFLICTS OF INTEREST

The authors declare that they have no conflicts of interest.

REFERENCES

[1] Z. Duan, T. Wu, S. Guo, T. Shao, R. Malekian, and Z. Li, "Development and trend of condition monitoring and fault diagnosis of multi-sensors information fusion for rolling bearings: A review", *International Journal of Advanced Manufacturing Technology*, vol. 96, pp. 803–819, 2018. DOI: 10.1007/s00170-017-1474-8.

[2] M. D. Wagh, S. B. Puneeth, S. Goel, and S. K. Sahoo, "Development of laser-induced graphene-based automated electro microfluidic viscometer for biochemical sensing applications", *IEEE Transactions on Electron Devices*, vol. 68, no. 10, pp. 5184–5191, 2021. DOI: 10.1109/TED.2021.3107374.

[3] L. V. Markova, V. M. Makarenko, M. S. Semenyuk, and A. P. Zozulya, "On-line monitoring of the viscosity of lubricating oils", *Journal of Friction and Wear*, vol. 31, pp. 433–442, 2010. DOI: 10.3103/S106836661006005X.

[4] A. V. Mirgorodskaya, "The history of the development of the capillary method for measuring kinematic viscosity: From the Lomonosov viscometer to the information-measuring system", *Measurement Techniques*, vol. 66, pp. 610–618, 2023. DOI: 10.1007/s11018-023-02273-y.

[5] J.-L. Daridon, J.-P. Bazile, and G. Galliero, "Advances in falling-cylinder viscometry: A comprehensive review", *International Journal of Thermophysics*, vol. 45, art. no. 71, 2024. DOI: 10.1007/s10765-024-03356-w.

[6] T. Hirano, S. Mitani, and K. Sakai, "Development and progress of innovative rotational-type viscometer with electromagnetically spinning method", *Nihon Reoroji Gakkaishi*, vol. 46, pp. 53–58, 2018. DOI: 10.1678/rheology.46.53.

[7] A. Abdulkareem, U. Erturun, and K. Mossi, "Non-destructive evaluation device for monitoring fluid viscosity", *Sensors*, vol. 20, no. 6, p. 1657, 2020. DOI: 10.3390/s20061657.

[8] X. Zhu C. Zhong, and J. Zhe, "Lubricating oil conditioning sensors for online machine health monitoring – A review", *Tribology International*, vol. 109, pp. 473–484, 2017. DOI: 10.1016/j.triboint.2017.01.015.

[9] F. Yan and H. L. W. Chan, "Analytical model of piezoelectric cantilever as rheological sensor", *Physica B: Condensed Matter*, vol. 406, no. 19, pp. 3605–3608, 2011. DOI: 10.1016/j.physb.2011.06.052.

[10] F. Ju and S.-F. Ling, "Sensing fluid viscosity and density through mechanical impedance measurement using a whisker transducer", *Measurement Science and Technology*, vol. 24, no. 5, art. no. 055105, 2013. DOI: 10.1088/0957-0233/24/5/055105.

[11] X. Lu, L. Hou, L. Zhang, Y. Tong, G. Zhao, and Z. Y. Cheng, "Piezoelectric-excited membrane for liquids viscosity and mass density measurement", *Sensors and Actuators A: Physical*, vol. 261, pp. 196–201, 2017. DOI: 10.1016/j.sna.2017.05.014.

[12] T. Yanaseko, H. Sato, I. Kuboki, K. Mossi, and H. Asanuma, "Vibration viscosity sensor for engine oil monitoring using metal matrix piezoelectric composite", *Materials*, vol. 12, no. 20, p. 3415, 2019. DOI: 10.3390/ma12203415.

[13] H. Yu, L. Liang, and A. G. Yuandong, "Capacitive micromachined ultrasonic transducer (CMUT) based micro viscosity sensor", *Sensors and Actuators B: Chemical*, vol. 227, pp. 346–351, 2016. DOI: 10.1016/j.snb.2015.12.061.

[14] M. Schirru, X. Li, M. Cadeddu, and R. S. Dwyer-Joyce, "Development of a shear ultrasonic spectroscopy technique for the evaluation of viscoelastic fluid properties: Theory and experimental validation", *Ultrasonics*, vol. 94, pp. 364–375, 2019. DOI: 10.1016/j.ultras.2018.07.002.

[15] S. Esmaeili and J. R. Shahrouzi, "A microcantilever-based viscometer for inline determination of liquid viscosity", *Engineering Research Express*, vol. 7, art. no. 015005, 2025. DOI: 10.1088/2631-8695/adabba.

[16] L. Liu, D. Hu, and R. H. W. Lam, "Microfluidic viscometer using a suspending micromembrane for measurement of biosamples", *Micromachines*, vol. 11, no. 10, p. 934, 2020. DOI: 10.3390/mi11100934.

[17] Z. Abbassi, A. Benabdellah, M. Adar, Y. Najih, and A. Nakheli, "Electromagnetic penetrometer for high viscosity measurement using a new displacement sensor", *Sensors and Actuators A: Physical*, vol. 380, art. 116018, 2024. DOI: 10.1016/j.sna.2024.116018.

[18] A. D. Gomes, J. Kobelke, J. Bierlich, K. Schuster, H. Bartelt, and O. Frazao, "Optical fiber probe viscometer based on hollow capillary tube", *Journal of Lightwave Technology*, vol. 37, no. 18, pp. 4456–4461, 2019. DOI: 10.1109/JLT.2019.2890953.

[19] T. Basumatary, D. Chetia, H. K. Singh, and T. Bezboruah, "Fiber optic viscometer based on sliding of liquid drop under gravity on inclined flow channel", *IEEE Transactions on Instrumentation and Measurement*, vol. 65, no. 4, pp. 930–938, 2016. DOI: 10.1109/TIM.2016.2516259.

[20] Y. Bie, X. Guo, P. Song, J. Yang, and Z. Li, "A novel design of flow structure model for online viscosity measurement", *Insight*, vol. 61, no. 1, pp. 9–14, 2019. DOI: 10.1784/insi.2019.61.1.9.

[21] R. Mathew and A. R. Sankar, "Temperature drift-aware material selection of composite piezoresistive micro-cantilevers using Ashby's methodology", *Microsystem Technologies*, vol. 27, pp. 2647–2660,

2021. DOI: 10.1007/s00542-020-05013-2.
[22] Anton Paar GmbH. [Online]. Available: https://www.anton-paar.com/corp-en/products/details/svm-series/?sku=105013
[23] Delite (Beijing) Technology Co., Ltd. [Online]. Available: https://www.delite.com.cn/A1010yd.html
[24] Changji Geological Instrument Co., Ltd. [Online]. Available: https://www.shangyi.net/index.php?m=view&a=index&aid=296&cid=79
[25] Beijing TimePower Measure and Control Equipment Co., Ltd. [Online]. Available: http://www.timepower.cn/products/zdydzd.html